JMEPEG (2009) 18:990–998
DOI: 10.1007/s11665-008-9329-y

1059-9495/$19.00

High Power Diode Laser Surface Treatment to Minimize Droplet Erosion of Low Pressure Steam Turbine Moving Blades

B.S. Mann, Vivek Arya, B.K. Pant, and Manish Agarwal

(Submitted March 8, 2008; in revised form October 10, 2008)

This article deals with the high power diode laser (HPDL) surface treatment to overcome water droplet erosion of Low Pressure Steam Turbine (LPST) moving blades used in high rating conventional, critical and super critical thermal power plants. The materials generally used in these steam turbines are titanium alloy (Ti6Al4V), precipitate hardened stainless steel (17Cr-4Ni PH), X20Cr13 and X10CrNiMoV1222 steels. During incubation period as well as under prolonged testing, the HPDL surface treatment of these materials except for 17Cr-4Ni PH steel has enhanced the droplet erosion resistance significantly. This is due to increased hardness and formation of fine-grained martensitic phase due to rapid heating and cooling rates associated with laser treatment. The droplet erosion results of HPDL laser surface treatment of all these materials and their analysis form the main part of the article.

Keywords control valve, diode laser, LP bypass valve, stainless steel, steam turbine, titanium alloy, water droplet erosion

1. Introduction

Despite tremendous developments in low pressure steam turbine (LPST) moving blade design and blade materials, the water droplet erosion of blades still remains an unsolved problem. This problem becomes more severe for high rating (500 MW), critical and supercritical (600 and 800 MW) steam turbine moving blades due to their large size. To remove higher level of moisture, the last row of stationary blades is provided with suction slots, moisture is removed from the blade path and drained into the condenser. Alstom Power, GE Power, and Siemens Power Generation have started using LP steam turbine blades of size up to 56″ (1422.4 mm). Mitsubishi Heavy Industries Ltd. is working on introducing 74″ (1880.0 mm) low pressure titanium alloy blades for their high rating supercritical steam turbines. (1371 MW). When these blades rotate at 50 Hz they produce tip velocities more than 750 m/s, which is detrimental to the blade material due to very high impact energy of the water droplets. In applications where moisture level is still high, Siemens employs steam heating to minimize the formation of water droplets (Ref 1). Alstom Power and GE Power use titanium alloy where there is risk of water droplet erosion and also use water extraction through hollow stationary blades and provide water removal channels (Ref 2). Still there are chances that droplets of size greater than 200 microns may form. These can quickly erode the moving blades (Ref 3). Similar droplet sizes occur in high rating and supercritical steam turbines though the data in the literature are not available. Material loss from the leading edge of these blades is the result of the cumulative impact of water droplets. At present the leading edges of LPST blades (X20Cr13 and X10CrNiMoV1222 steels) are hardened by using conventional hardening techniques (flame or high frequency induction hardening) followed by rapid water quenching. For erosion prediction, Krzyzanowski and Szperngiel proposed the formula which is given as below (Ref 4).

$$U_{eMD} = \frac{U_a}{N_e}\left(\frac{W * N}{2550}\right)^{4.92}\left(\frac{d^*}{10^{-3}}\right)^{1.69} \quad \text{(Eq 1)}$$

U_{eMD} represents maximum material volume loss per unit area per unit time
U_a represents total volume of water impinging on the unit blade surface element per unit time
$W * N$ represents normal velocity component
d^* represents droplet size
N_e represents normalization with respect to 18-8 stainless steel.

This equation gives maximum instantaneous value of the material volume loss per unit area per unit time. The droplet structure was assumed to be homogeneous and the angle of attack was about 90 degree. In the present study, the theoretical prediction for erosion damage estimation based upon the preceding equation has been carried out. All the parameters such as energy flux, mass flux, impingement angle, droplet size, and velocity were considered while comparing with the actual steam turbine conditions.

Laser hardening is an excellent protection method against droplet erosion; however, it introduces both compressive as

B.S. Mann, Vivek Arya, B.K. Pant, and **Manish Agarwal**, Surface Coatings and Treatment Laboratory, BHEL, Corporate R&D Division, Vikasnagar, Hyderabad 500093, India. Contact e-mail: balbir@bhel rnd.co.in.

well as tensile residual stresses in the material. Austenite phase retention resulting in volume decrease gives rise to the tensile stresses, whereas martensitic transformation causes volume increase and gives rise to compressive residual stresses in steels (Ref 5). The distribution of these stresses largely depends upon geometry of the blades as well as on the heating and cooling rates of the laser-hardened layer. These residual stresses in the laser treated layer on a rectangular Gr. 500-7 steel specimen in the direction of laser beam are reported to cause convex bending which result in increased tensile residual stresses and range from +50 to +200 MPa, whereas across the laser beam these are always compressive and generally range between −5 to −80 MPa (Ref 6). The excessive stresses on the laser-hardened surface may initiate cracks which may propagate into the blade material causing failure.

In the present study deflections occurring during high power diode laser (HPDL) surface treatment in the martensitic stainless steel X10CrNiMoV1222 as well in Ti6Al4V alloy on rectangular samples were measured using 3-D coordinate measurement machine. The residual stresses that arose due to these deflections were validated on X10CrNiMoV1222 steel samples using X-ray Residual Stress Analyzer. These results along with analysis of HPDL surface treated layers using scanning electron microscope and evaluation of droplet erosion resistance using liquid impingement erosion as per ASTM G-73-98 are reported in this article.

Siemens, Alstom, and GE Power have started using titanium alloy for LPST moving blades of size up to 56″ (1422.4 mm) for their high rating steam turbines where the risk of water droplet erosion is much more. In addition to LPST moving blades, the droplet erosion is a significant problem in the control valves and LP bypass valves, generally on the inner side of the casing (Ref 7, 8). The material generally used for the casing is X10CrMo910 (0.14C, 0.28Si, 0.65Mn, 2.4Cr, 0.91Mo, P&S <0.014 bal. Fe). Significant corrosion in combination with droplet erosion in control valves is due to the formation of larger droplets impinging at high speed exceeding 240 m/s. HPDL surface treatment is likely to be beneficial for titanium alloy, X20Cr13, X10CrMo910, and X10CrNiMoV1222 steels for this problem.

1.1 High Power Diode Laser Surface Treatment

Surface modification of martensitic stainless AISI 420 steel using a 3.5 kW continuous wave CO_2 laser has been reported (Ref 5, 9). The cavitation erosion resistance of laser melted specimens using a CO_2 laser at a power of 1.7 kW and at a scanning speed of 25 mm/s was reported to be 70 times better than untreated AISI 420 steel (Ref 5). The excellent cavitation erosion resistance was due to the combined effect of a high volume fraction of retained austenite (89%) and moderate hardness (450 Hv). This phase has an excellent characteristic of absorbing water impact shocks and subsequently transforming in situ to a martensitic phase (Ref 5). The conversion of austenitic phase into martensitic phase induces compressive stresses on the surface, which are beneficial to overcome impingement erosion. On the other hand, it is also reported that the cavitation erosion resistance increases with the increase in hardness up to a maximum value and then dropped with further increase in hardness.

Laser hardening studies were limited to a narrow power density in the range of 1740-2400 W/(cm^2/s). Cavitation and droplet erosion phenomenon are similar and some of the experimental findings on laser hardening of 12Cr steel using CO_2 laser in droplet erosion are already available in the literature (Ref 9-11). However, the information on droplet erosion and their damage mechanism phenomenon using HPDL treatment, for these steels and titanium alloy are not available.

2. Experimental

2.1 HPDL Surface Treatment

Droplet erosion samples of size 12.7 mm Ø × 40 mm length having internal threading M8 were made from each of the materials typically used in steam turbines including titanium alloy Ti6Al4V, 17Cr-4Ni PH, X20Cr13, and X10CrNi-MoV1222 stainless steels. 17Cr-4Ni PH steel was laser-hardened in as-received condition (not precipitation hardened). A fixture was fabricated to hold and rotate these samples while carrying out HPDL surface treatment. Each sample was fixed in a self-centered three jaw chuck at one end and supported on a fixture on the other end. The fixture has a rotating seal, so that the samples can rotate freely and air used for cooling the samples does not leak. Rapid cooling of the sample was carried out during HPDL treatment by introducing compressed air having volumetric flow rate of 15-16 m^3/h through the M8 tapped hole. This air is capable of removing heat at a rate of 160-180 W, which is comparable to the heat removed in a bulk stainless steel and titanium alloy during laser surface treatment. The samples were thoroughly cleaned using acetone before the start of the experiment to make the surface free from dust, oil, etc. The complete setup is shown in Fig. 1.

High power diode laser surface treatment was carried out on each sample using 4.6 kW Diode Laser System (Laserline, GmbH). The laser head was mounted on a six plus two axis robot (Kuka, GmbH). Optics of '30 mm × 3.0 mm' was used to produce the laser beam at focal length of 275 mm. Laser beam power was controlled in a closed loop by a two color pyrometer and a uniform surface temperature of 1550 °C was maintained. The complete system was controlled by the Robot controller. The robot was programed in such a way that the laser beam tracked the sample at a speed ranging from 5 to 15 mm/s ensuring that hardening of the sample was completed in one pass. Thus a wide area having a span of 30 mm on the outer

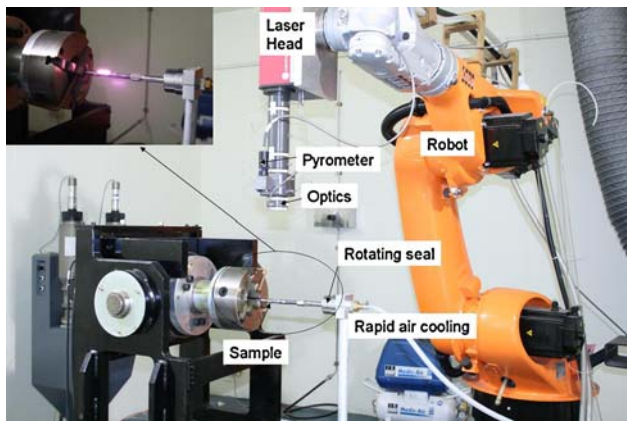

Fig. 1 Showing complete set up for doing HPDL surface treatment. (Inset: HPDL treatment being carried out on the sample)

periphery of the sample was laser hardened in one pass. The uniform compressed air cooling of the sample was maintained throughout the HPDL treatment process. The HPDL treatment of each sample was completed in 8 s. The typical power density used for the surface treatment of round samples was in the range of 770-1150 W/(cm^2/s) where as for rectangular flat samples was in the range of 1150-1620 W/(cm^2/s) for a surface temperature of 1550 °C. Lower power density is for titanium alloy and higher for steel samples. This is due to the difference in their thermal diffusivities. The HPDL power density is much lower than that of CO_2 laser used earlier on rectangular samples for similar treatment because of better absorption of diode laser on the materials as compared to CO_2 laser (Ref 5, 10).

2.2 Conventional Heat Treatment of X20Cr13 Steel

Conventional heat treatment was carried out on X20Cr13 steel samples (LPST blade material) to make a comparison with the HPDL treated sample. Precisely controlled heating of these samples was carried out at a temperature of 980 ± 5 °C in an electric furnace followed by oil quenching to achieve hardness in range of 450-500 HV, which is generally obtained either by flame or high frequency induction hardening techniques. These samples along with the HPDL surface treated X20Cr13 steel samples were studied for droplet erosion to evaluate the efficacy of HPDL treatment over conventional heat treatment.

2.3 Droplet Erosion Testing of HPDL Surface Treated Samples

The details of droplet erosion test facility are given in Ref 9-11. In short, the test facility consists of a 700-mm diameter chamber and a round stainless steel disk where the test samples are positioned. Samples, 40 mm in length and 12.7 mm in diameter are affixed on the periphery of the disk. The disk is rotated at 79.166 cycles/s to obtain the test sample tangential velocity of 147.0 m/s. Two water jets impinge on the cylindrical test samples and cause impingement erosion. As such, a relative velocity of 147.6 m/s is obtained. The mass of water impacted from the jets per cycle is 0.023 mL and 0.035 mL equivalent to energy flux values of 37.158×10^6 J/m^2 s and 57.167×10^6 J/m^2 s, respectively. The details of the test set up are given in Fig. 2 and experimental values of test parameters are given in Table 1. Siemens have also carried out similar studies on X20Cr13 steel using 800 micron droplets impinging at a velocity of 300 m/s corresponding to impact energy of 0.012 J (Ref 12). In the present study, more accelerated conditions corresponding to impact energy levels of 0.25 J and 0.38 J were adopted to obtain the result in a short duration on different materials.

The cylindrical specimens were selected because the impingement erosion occurs at the leading edge of actual steam turbine blades, which also have similar leading edge radii

Table 1 Experimental test conditions

Conditions	Test I	Test II
Volume of water impacted per cycle	0.023 mL	0.035 mL
Water impact energy, 1/2 mV^2	0.250 J	0.380 J
Water energy flux, J/m^2 s	37.158×10^6	57.167×10^6
Water mass flux	3.44 m/s	4.0 m/s
Relative water velocity	147.6 m/s	147.6 m/s
Test sample size	φ 12.70 × 40 mm	φ 12.70 × 40 mm
Number of specimens used	12	12
Test duration cycles	13.176×10^6	3.0195×10^6
Angle of impact	0-90°	0-90°
Impact frequency	79.166 cycles/s	79.166 cycles/s
Experimental accuracy	±15.5%	±15.5%

Water droplet impact energy (1/2 mV ^{2}) in actual steam turbines for typical 800 micron droplet size at 300 m/s is .0125 J and at 750 m/s is 0.075 J

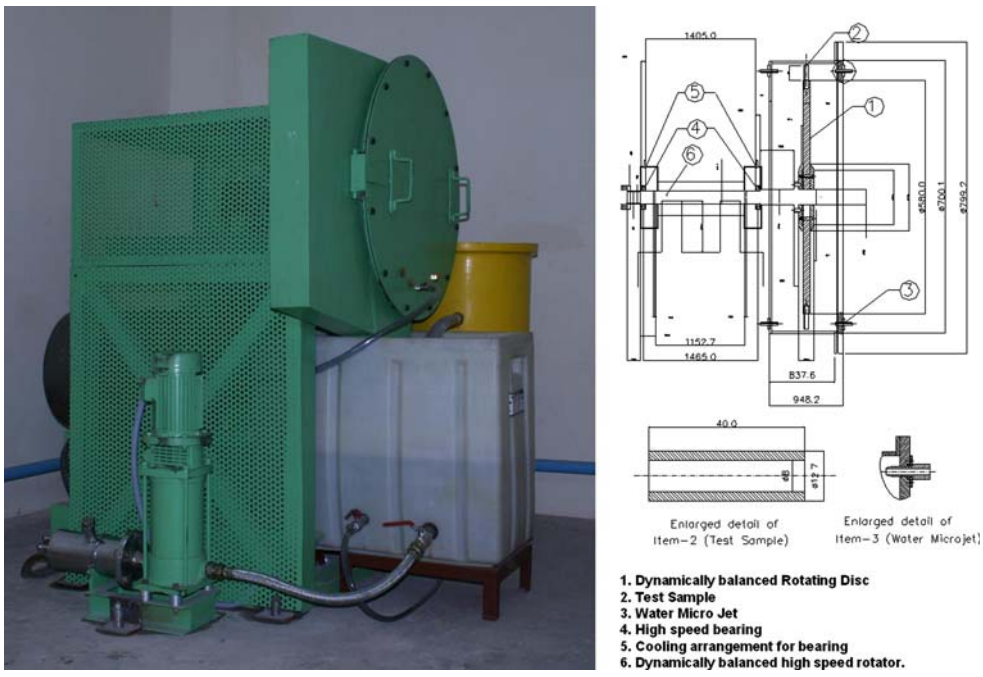

Fig. 2 Water droplet impingement erosion test facility

Table 2 Materials used for droplet erosion testing

Materials	Composition (wt.%)	
Ti6Al4V	6Al, 4V	Bal Ti
X20Cr13	0.20C, 0.5Si, 0.5Mn,13Cr, 0.5Ni	Bal Fe
X10CrNiMoV1222	0.1C, 0.25Si, 0.7Mn, 12Cr, 2.5Ni, 1.75Mo, 0.3V	Bal Fe
17Cr-4Ni PH	0.06C, 15.67Cr, 0.27Si, 0.64Mn, 4.25Ni, 3.6Cu, 0.19Nb	Bal Fe

as that of the test samples. A precision balance (±0.1 mg) was used for measurement of mass loss after testing. The test duration depending upon energy and mass fluxes was selected in such a way as to achieve steady-state erosion in limited cycles. The accuracy and repeatability of the test have been established on X20Cr13 steel sample which is taken as a reference material. The extent of erosion damage is calculated from the mass loss divided by the density of the material. The results have been plotted in the form of cumulative volume loss versus number of cycles. Table 2 gives the materials used for HPDL treatment and for droplet erosion evaluation.

The Vicker's micro hardness of HPDL treated and untreated samples was measured by using Tukon 2100 Macro/Micro hardness tester (Wolpert, USA) by applying a load of 300 g with a dwell time of 13 s. The X-ray diffraction (XRD) of HPDL surface treated steels and titanium alloy samples were taken using Philips X-pert system (Philips, Netherlands). The residual stress measurements on HPDL treated samples were carried out using X-ray Residual Stress Analyzer (StressTech, USA).

3. Results and Discussion

3.1 Droplet Erosion Damage Mechanism and Test Results

Erosion caused by liquid droplet impact has similarities to that arising due to cavitation bubble collapse. The details of erosion damage mechanism for a particular material due to cavitation or liquid droplet impact are given in Ref 13, 14. In brief the cavitation process is under stood as (i) the formation of local vapor pockets inside a liquid due to increase in velocity or drop in pressure of sufficient magnitude (ii) the vapor pockets may take the form of small bubble or many bubbles (iii) These bubbles are transported downstream to collapse in a high pressure region (iv) those which collapse on or near a solid boundary produce high energy impacts on the surface. The forces causing this deformation and erosion are micro jet impacts occurring when the bubbles collapse. In addition to micro-jets, high pressure shock waves are also generated which weakens the materials. Erosion is mainly caused by micro jet impacts arising due to bubble collapse similar to that caused by liquid droplet impact. For enhancing droplet or cavitation erosion resistance of materials, retention of austenitic phase is highly beneficial because it is transformed into hard martensitic phase during the prolonged process of droplet or cavitation erosion. The austenitic phase being soft may get removed even before its transformation. Hence, an optimum balance of both martensitic and austenitic phases is essential for good cavitation/droplet erosion properties. However, in our case the improvement in droplet erosion resistance is not due to in situ austenite to martensite transformation but mainly due to fine-grained microstructure after laser treatment.

For comparing the erosion damage (cumulative volume loss) at both the impact energy levels of 0.25 J and 0.38 J, the formula given by Krzyzanowski and Szperngiel (Ref 4) has been used. The extent of damages occurring at the above energy levels agrees with the predictions made from the above formula. Later on our experimental damage values were compared with the actual impact energy levels occurring in conventional steam turbines typically at 300 m/s for 800 micron droplet (0.012 J) and in supercritical steam turbines typically at 750 m/s for 800 micron droplet (0.075 J). The damages occurring due to droplet erosion in nuclear power plants may be more aggressive due to excessive wetness of the steam (13%) (Ref 15). Our experimental impact energy level (0.38 J) is approximately 5 times more than the actual maximum field condition values and is capable of producing more severe damage.

The droplet erosion test results of different HPDL surface treated and untreated samples are given in Fig. 3 and 4. The performance of all the materials except 17Cr-4Ni PH steel after laser surface treatment has improved manifold. It is seen from the figures that excellent performance is given by HPDL surface treated X20Cr13 steel followed by X10CrNiMoV1222 steel and Ti6Al4V alloy for both the energy flux levels (37.158×10^6 J/m^2 s and 57.167×10^6 J/m^2 s).

After an operation of 0.855×10^6 cycles at an energy flux of 57.167×10^6 J/m^2 s, the maximum improvement has been observed for X20Cr13 steel (approximately 54 times). However, at lower energy flux of 37.158×10^6 J/m^2, even after prolonged duration, infinite times improvement has been observed for this material (zero volume loss, refer Fig. 3). After laser surface treatment this material has achieved highest hardness compared to the hardness achieved for other materials (Table 4). This is followed by X10CrNiMoV1222 steel (8.5 times improvement after an operation of 1.14×10^6 cycles at an energy flux of 57.167×10^6 J/m^2 s). For titanium alloy, under similar conditions this improvement is approximately 5.3 times. It can also be seen that droplet erosion resistance of X10CrMo910 steel used in LP bypass valves, after HPDL treatment, has improved 12.5 times at energy flux of 37.158×10^6 J/m^2 s and 7.7 times at 57.167×10^6 J/m^2 s, respectively. There is no improvement in droplet erosion resistance for 17Cr-4Ni PH steel after HPDL treatment because there is no improvement in its micro hardness. It is also observed from the Fig. 3 and 4 that the droplet erosion resistance of untreated X10CrNiMoV1222 steel at both energy levels lies between X20Cr13 and 17Cr-4Ni PH steel although the mechanical properties including modified resilience of this steel are much better than X20Cr13 and comparable to 17Cr-4Ni PH steel (Ref 11). This could have happened due to reduced martenstic phase in X10CrNi-MoV1222 steel compared to X20Cr13 steel after HPDL treatment. Using XRD the austenitic phase could not be detected in X10CrNiMoV1222 steel (Fig. 5).

Droplet erosion tests on "heat treated" X20Cr13 samples (which is presently adopted for LPST blades) were also carried out. From Fig. 4 it can be seen that its performance is much inferior to laser-hardened X20Cr13. (Volume loss of 10.17 mm^3 compared 2.98 mm^3 at an energy flux of 57.167×10^6 J/m^2 s after an operation of 2.196×10^6 cycles). The trend of laser-hardened X20Cr13, X10CrNiMoV1222, and Ti6Al4V materials in droplet erosion at both energy flux levels is the same. However, their magnitude of damages is different.

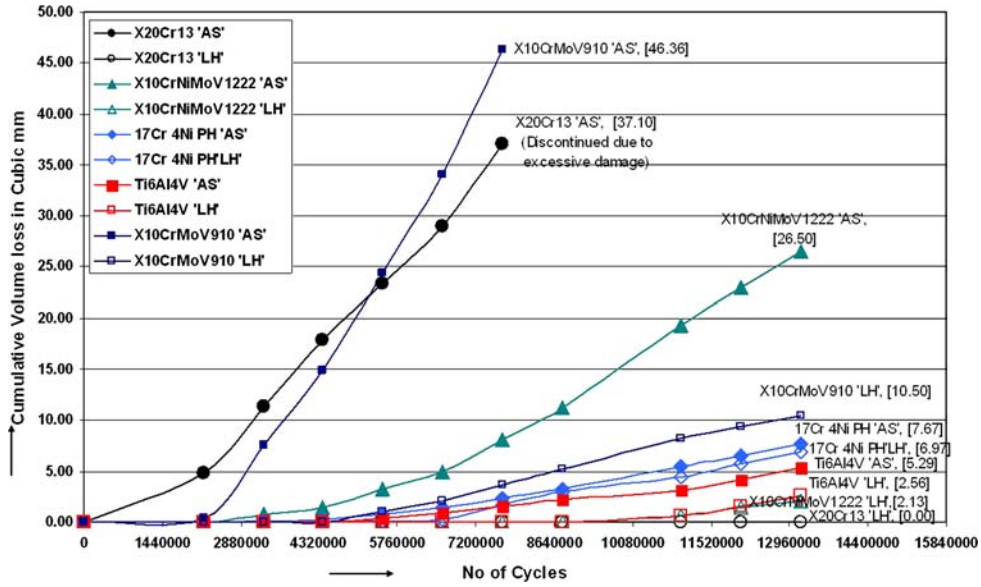

Fig. 3 Volume loss of different materials after HPDL hardening at an energy flux of 37.158×10^6 J/m^2 s

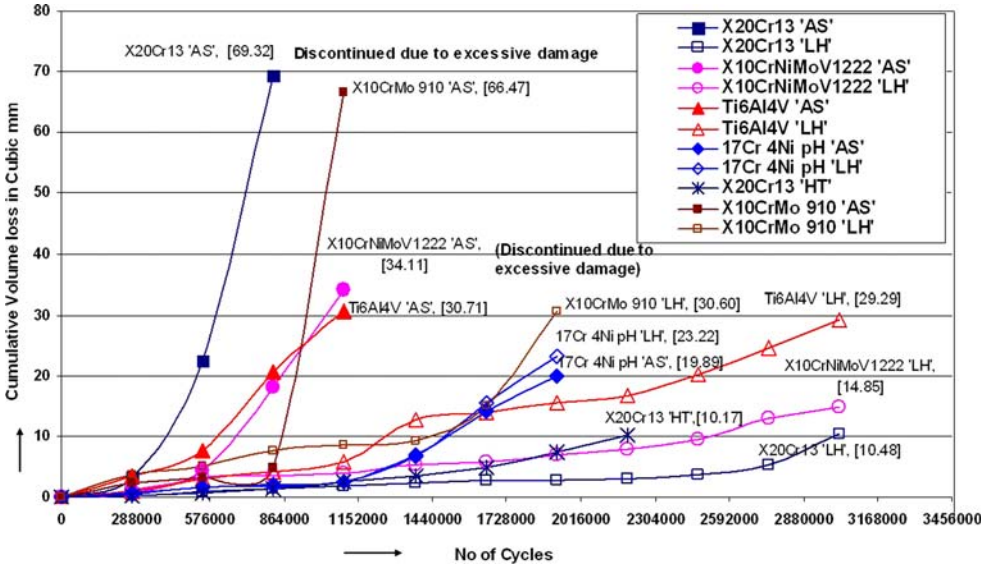

Fig. 4 Volume loss of different materials after HPDL hardening at an energy flux of 57.167×10^6 J/m^2 s

Different materials have different heating/cooling rates which depends upon their thermal diffusivity. The microstructure after laser treatment of the materials also depends on the thermal diffusivity. The thermal diffusivity of the candidate materials chosen lie in the descending order, i.e., X20Cr13, 17Cr 4Ni PH, X10CrNiMoV1222, and Ti6Al4V. All the steels get quenched from above AC_1 at different rates, whereas the Ti6Al4V alloy undergoes a phase change at around 880 °C. X20Cr13 steel has the highest quenching rate (thermal diffusivity) and hence a resultant microstructure of very fine-grained martensite. This fine-grained martensite is responsible for high hardness and best droplet erosion resistance.

Analysis of tap water used for testing of the materials is given in Table 3. The concentration of salts in the water was more than that in the tests conducted earlier (Ref 9-11). This has resulted in comparatively more severe damage of the materials; however, their trend and performance are similar. There were salt deposits on and inside the samples which have resulted in slight increase in weight during incubation period. Necessary corrections were made to account for this error.

3.2 Scanning Electron Micrographs

The scanning electron micrographs of eroded samples are shown in Fig. 6-8. From the SEM of HPDL treated X20Cr13 steel sample, it can be seen that there are several micro cracks visible in the hardened region, whereas there are no cracks seen in the unhardened sample. This indicates that the material removal due to droplet erosion after HPDL treatment for this material is brittle in nature. Also, from the exposed microstructures it is seen that the grain size is much smaller for all the laser treated materials as compared to the untreated materials

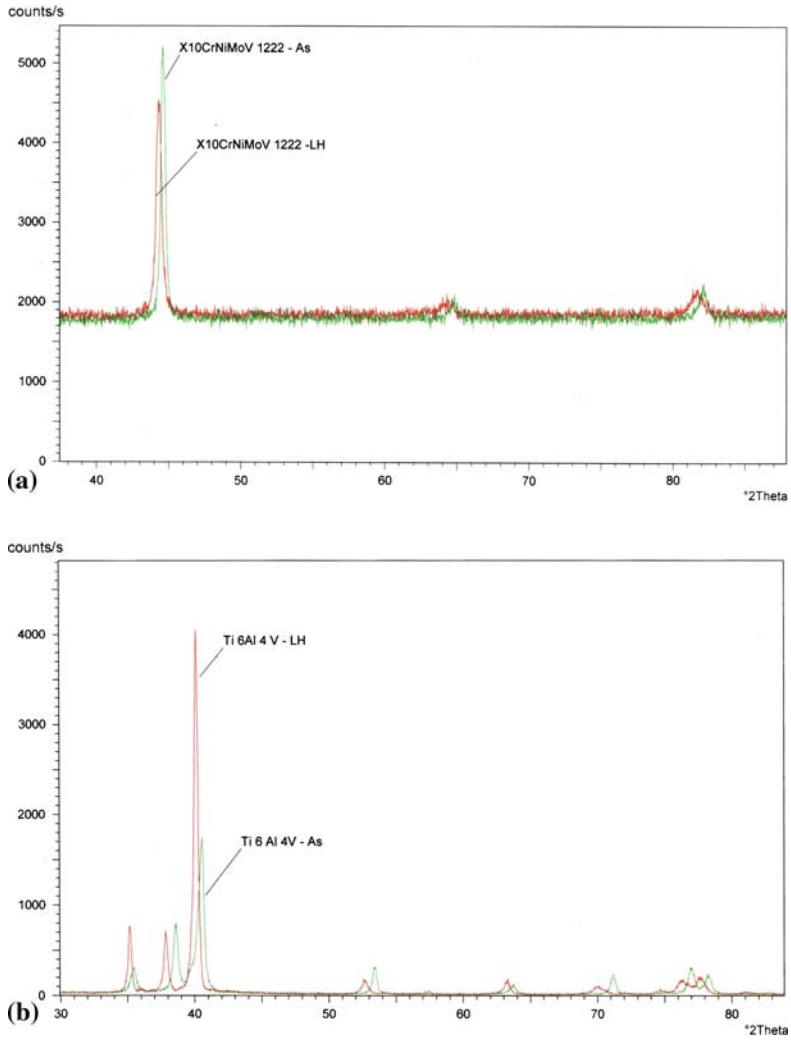

Fig. 5 Figures show X-ray diffraction patterns of HPDL treated and untreated X10CrNiMoV1222 steel (a) and Ti6Al4V alloy (b), respectively

Table 3 Water analysis report

Parameter	Units	As per Ref 10	Present study
pH		6-7	6-7
Conductivity	Millimhos/cm	0.887	1.176
Total hardness	ppm	400	598
Calcium hardness	ppm	196	306
Magnesium hardness	ppm	204	292
M-Alkalinity	ppm	240	320
P-Alkalinity	ppm	Traces	Traces
Chlorides	ppm	102	102
Sulfates	ppm	29	70
Total solids	ppm	780	1160

(Fig. 6-8). It is also observed that, after long exposure deep micro tunnels conforming to micro jetting effects similar to cavitation erosion mechanism are observed in all the laser treated samples. Scanning electron micrographs showing micro jetting effects for only X10CrNiMoV1222 steel are reported in this article (Fig. 8a, b).

3.3 Micro Hardness Values

It is seen from Table 4 that maximum increase in hardness was observed for HPDL treated X20Cr13 steel followed by X10CrNiMoV1222, whereas there was only a marginal increase in the micro hardness for titanium alloy and there was no improvement for 17Cr-4Ni PH steel.

3.4 X-ray Diffraction Test Results

X-ray diffraction details for X10CrNiMoV1222 steel and titanium alloy are only reported in this article (refer Fig. 5). XRD using copper K alpha radiation and nickel filter were used in the present study and investigations were carried in a similar way as reported in Ref 5. XRD analysis of X10CrNiMoV1222 steel confirms the presence of martensitic phase only, retained austenitic phase in this steel could not detected or may be below the detection limits of XRD (refer Fig. 5). This along with reduced micro hardness may be one of the main reasons for its lower droplet erosion resistance as compared to X20Cr13 steel. Information on the retention of austenitic phase in AISI 420 as well as 13Cr-4Ni steel samples after laser treatment is already available in the literature (Ref 5, 16). Retention of

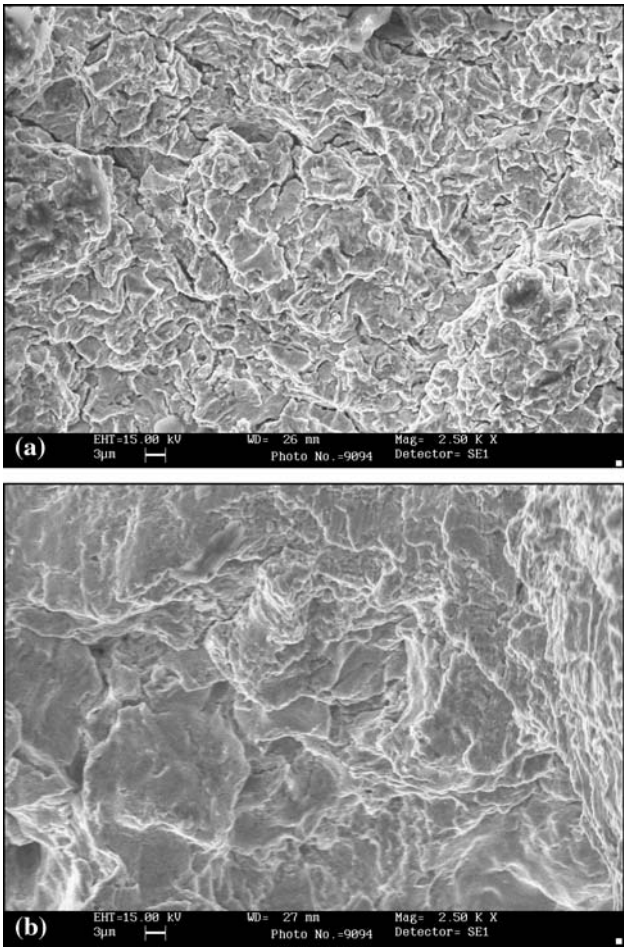

Fig. 6 Figures show SEM micrographs of droplet impingement eroded HPDL treated X20Cr13 steel after 570,000 cycles (a) and untreated X20Cr13 steel after 285,000 cycles (b), respectively, at energy flux of 57.167×106 J/m^2 s

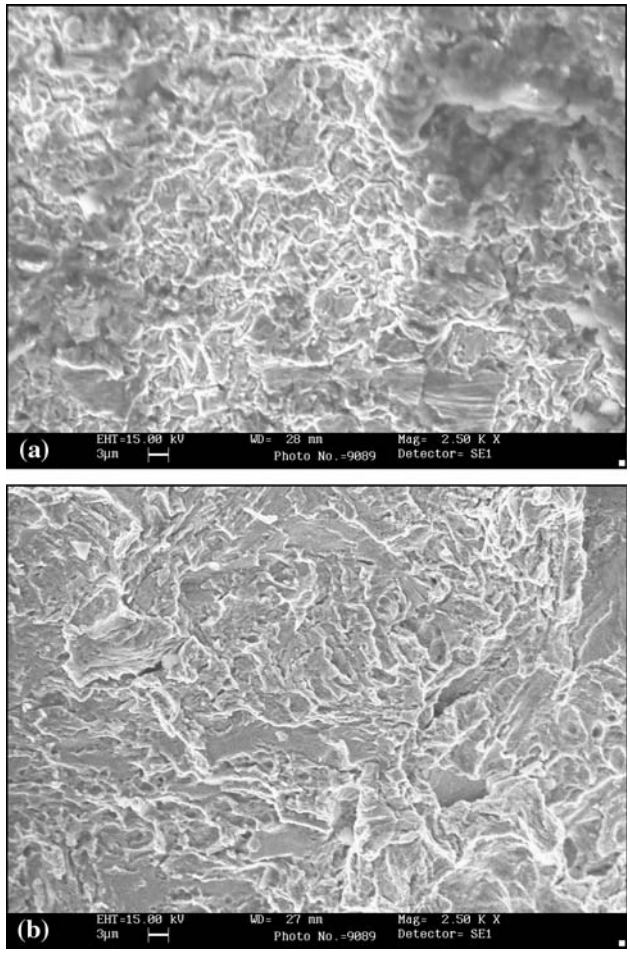

Fig. 7 Figures show SEM micrographs of droplet impingement eroded HPDL treated X10CrNiMoV1222 steel after 570,000 cycles (a) and untreated X10CrNiMoV1222 after 285,000 cycles (b), respectively, at energy flux of 57.167×106 J/m^2 s

excessive austenitic phase for LPST moving blades may be detrimental as this leads to increased tensile stresses causing reduced fatigue life.

After laser hardening Ti6Al4V alloy has shown little change in hardness but has shown a remarkable improvement in the droplet erosion resistance at both the energy fluxes. From the XRD, it is seen that the alpha phase (HCP) has increased after laser treatment. This is apparent from the increase of alpha peaks at 2 theta values at 35 and 40 degrees and a reduction of beta peaks at 2 theta values at 37.8 and 69.8 degrees after laser hardening. This may be responsible for the improvement in the droplet erosion resistance.

3.5 Residual Stress Measurement

For residual stress measurements, flat titanium alloy and steel samples of size $100 \times 50 \times 6$ mm were used because the round samples have curvature and hence do not provide the correct values. The HPDL parameters such as the temperature of the sample and laser scan speed were the same on flat and round test samples. The measured residual stresses for X10CrNiMoV1222 flat sample lie in the range of −247.3 MPa (compressive) at the central portion of laser beam to +98.3 MPa (tensile) at the edge of the laser beam. The residual stress measurements were carried as per Ref 17. For titanium alloy the residual stresses using X-ray Residual Stress Analyzer could not be measured.

Deflections occurring during HPDL surface treatment in the martensitic stainless steels (X10CrNiMoV1222, X20Cr13, and 17Cr 4Ni PH) as well in Ti6Al4V alloy introduce residual stresses. The deflections at the central portion of the X10CrNiMoV1222 steel as well as titanium alloy were measured. The details of the deflections are given in Fig. 9. Maximum deflections were recorded at the central portion for titanium alloy around 430 micron, whereas for X10CrNiMoV1222 steel sample these deflections were around 200 micron. The radii of curvature arising due to deflections for steel as well as titanium alloy are also given in Fig. 9. It is seen from the Fig. 9 that the curvature for steel sample is concave across the laser beam resulting in compressive residual stresses and convex along the laser beam resulting in tensile residual stresses. Similar deflection and curvature trends were observed for flat rectangular ductile iron Gr. 500-7 sample while doing laser hardening as well as remelting using CO_2 laser. Moreover, the convection followed for measurement of curvature was different (Ref 18). On the other hand for titanium alloy, the curvature is concave in both the directions resulting in compressive residual stresses (Fig. 9). The deflections and hence the stresses developed in a

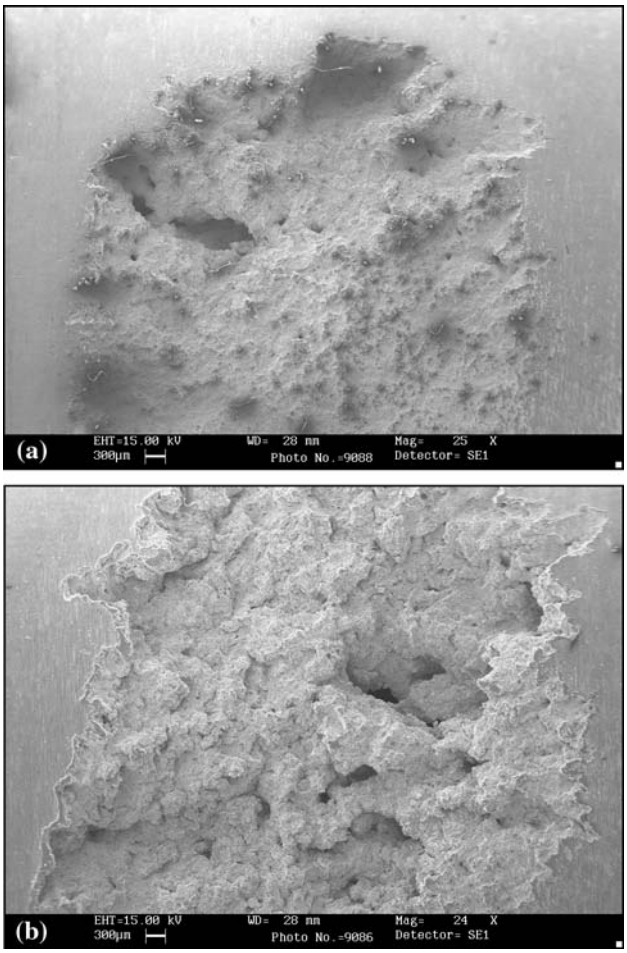

Fig. 8 Figures show SEM micrographs of droplet impingement eroded HPDL treated X10CrNiMoV1222 steel after 2,850,000 cycles (a) and untreated X10CrNiMoV1222 after 1,140,000 cycles (b), respectively, at energy flux of 57.167×106 J/m^2 s

Table 4 Micro hardness values of HPDL treated materials

Materials	Micro hardness before HPDL treatment, HV	Micro hardness after HPDL treatment, HV
X20Cr13	260-280	550-560
X10CrNiMoV1222	290-300	500-510
17Cr-4Ni PH	365-380	365-380
Ti6Al4V	330-350	360-380

particular material depend upon the geometry of the sample and its thermal response. For LPST moving blades these stresses may be different from the flat samples because the former have round leading edges. However their trends of being tensile in the direction of laser beam scan and compressive across the laser beam scan for steel will remain the same and for titanium alloy their trends of being compressive along and across the laser beam will remain unchanged. While adopting this technology on the LPST moving blades the actual stresses and retained austenitic phase may be measured. In case, these stresses are highly tensile in nature, they may be relieved by a heat treatment and should lie within the specified design limits.

4. Conclusions

Among X20Cr13, 17Cr-4Ni PH, X10CrNiMoV1222 steels and Ti6Al4V alloy, the HPDL treated X20Cr13 steel has given excellent performance in droplet erosion. This is followed by X10CrNiMoV1222 steels. Retained austenitic phase has not been observed in the X10CrNiMoV1222 steel. Reduced micro hardness may be one of the main reasons of their reduced performance in comparison to X20Cr13 steel.

In X20Cr13 steel after laser treatment, the micro cracks have appeared on the surface of the samples. These were not observed after long hours of testing (in the zone of deep erosion). These were also not observed in other steels and titanium alloy. For titanium alloy, although the micro hardness improvement after HPDL surface treatment is marginal, however, the improvement in droplet erosion under similar conditions is substantial. This may be due to excessive compressive stresses developed after HPDL treatment due to concave bending of the rectangular sample along and across the laser beam scan and increased alpha phase (HCP) after laser treatment.

From the SEM micrographs, it is seen that the grain size is much smaller for the laser treated materials as compared to the untreated ones and after long exposure, deep micro tunnels conforming to micro jetting effects similar to cavitation erosion mechanism are observed in all the materials studied. This confirms that the droplet erosion damage mechanism has a similarity to that of cavitation erosion.

For the same surface temperature, the power densities used for the HPDL surface treatment on round samples are found to lie in the range of 770-1150 W/(cm^2/s), whereas for rectangular samples in the range of 1150-1620 W/(cm^2/s). These values are much lower than those used in earlier studies on rectangular samples for similar surface treatment using CO_2 laser.

Presently droplet erosion shields using conventional hardening techniques are being adopted for LPST X20Cr13 and for X10CrNiMoV1222 moving blades. The HPDL surface treatment compared to conventional hardening has much improved droplet erosion resistance even at the highest impact energy of 0.38 J. The HPDL treated X20Cr13 steel is approximately three times better than the conventionally hardened steel. The HPDL surface treatment performance may be much improved at lower impact energy levels which are common in actual steam turbines (0.0125 J at 300 m/s and 0.075 J at 750 m/s for typical 800 micron droplet size).

After HPDL treatment, the flat samples of size $100 \times 50 \times 6$ mm have bent maximum up to 200-430 microns (lower values for X10CrNiMoV1222 steel samples and higher values for titanium alloy). The residual stresses in the central portion of the steel samples are highly compressive and change to tensile from the edge of the laser beam, whereas for titanium alloy these remain compressive as the curvature along and across the laser beam remains unchanged. These stresses could not be accessed along the depth.

In addition to LPST moving blades, the surface treatment using HPDL is one of the attractive solutions in the control valves and LP bypass valves to overcome droplet erosion problems which are inevitable.

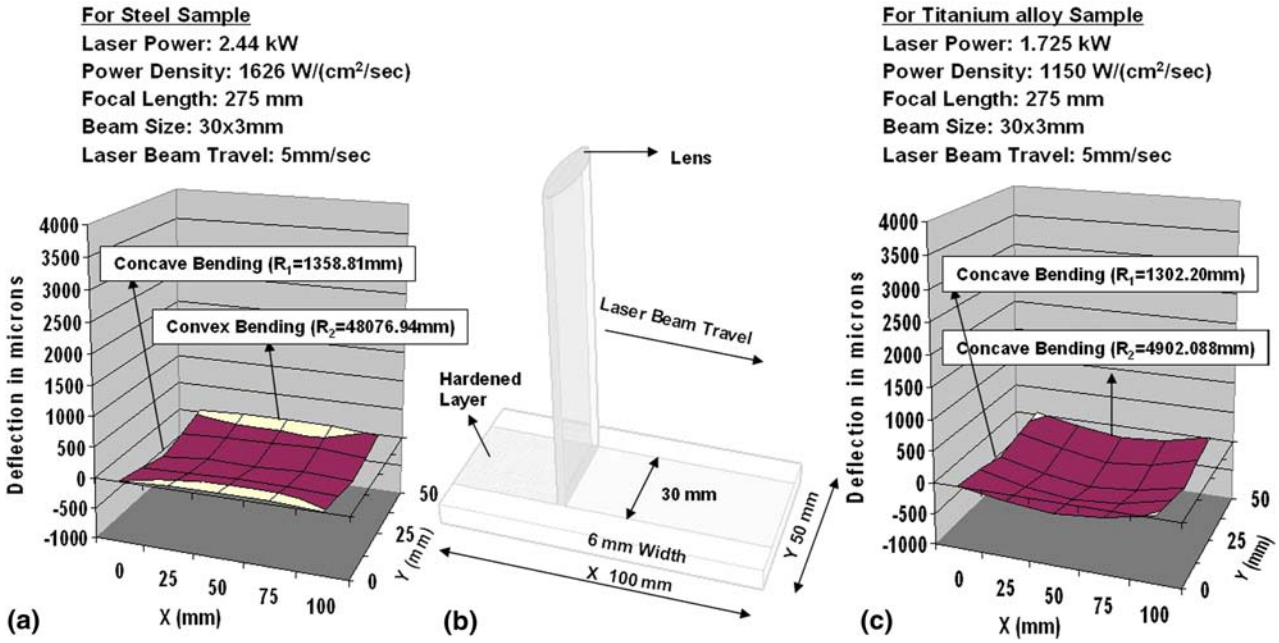

Fig. 9 Graph showing deflection in X10CrNiMoV1222 steel and Ti6Al4V alloy. (a) X10CrNiMoV1222 Steel, (b) Laser surface treatment, (c) Ti6Al4V alloy

Acknowledgments

The authors are thankful to Mr. V. Radhamohan for doing XRD analysis, Mr. Venkateswar Reddy for doing Scanning Electron Microscopy, and Mr. D. Vidyasagar for residual stress measurements. The authors are also thankful to the management of BHEL Corporate R&D for permission to publish this article.

References

1. J.R. Cheski, R. Patel, K. Rockaway, H. Osaghae, and M. Christianson, A Large Steam Turbine Retrofit Design and Operation History, *Presented at 2005 Power-Gen International Conference held at Las Vegas, N.V.* Dec 6–8, 2005, p 14
2. J.K. Reinker and P·B. Mason, Steam Turbines for Large Power Applications, GE Power System, GER-3646D, 1996
3. J. Krzyzanowski, The Correlation Between Droplet Steam Structure and Steam Turbine Blading Erosion, *J. Eng. Power*, 1974, **96**, p 256–266
4. J. Krzyzanowski and Z. Szperngiel, The Influence of Droplet Size on the Turbine Blading Erosion Hazard, *J. Eng. Power*, 1978, **100**, p 561–565
5. C.T. Kwok, H.C. Man, and F.T. Cheng, Cavitation Erosion and Pitting Corrosion Behaviour of Laser Surface Melted Martensitic Stainless Steel UNSS 42000, *Surf. Coat. Technol.*, 2000, **126**, p 238–255
6. J. Grum and R. Sturm, Residual Stresses State After the Laser Surface Remelting Process, *J. Mater. Eng. Perform.*, 2001, **10**(3), p 270–281
7. J. Kiesbauer, Control Valve for Critical Applications, *Hydrocarbon Process.*, 2001, **80**(6), p 89–100
8. S·V. Sherikar, Designing HRSG Desuperheaters for Performance Reliability, *Power*, 2006, **150**(2), p 1–7
9. B.S. Mann and V. Arya, An Experimental Study to Correlate Water Jet Impingement Erosion Resistance and Properties of Metallic Materials and Coatings, *Wear*, 2002, **253**, p 650–651
10. B.S. Mann and V. Arya, HVOF Coating and Surface Treatment for Enhancing Droplet Erosion Resistance for Steam Turbine Blades, *Wear*, 2003, **254**, p 652–667
11. B.S. Mann, V. Arya, and P. Joshi, Advanced HVOF Coating and Candidate Materials for Protecting LP Steam Turbine Blades Against Droplet Erosion, *J. Mater. Eng. Perform.*, 2005, **14**(4), p 487–494
12. W. Storch, G. Blum, B. Brenner, and G. Wiedemann, Laserhartung von Turbinenschaufelkanten, DK 621.165/620, Mitteilungen aus dem kraftwerk sanlagen, 1988, p 16–17
13. M.B. Lesser and J.E. Field, The Impact of Compressible Liquids, *Annu. Rev. Fluid Mech.*, 1983, **15**, p 97–122
14. W.F. Adler, The Mechanisms of Liquid Impact, in *Erosion*, C.M. Preece, Ed., Academic Press, New York, 1979, p 127–184
15. B. Stanisa, Z. Schauperl, and K. Grilec, Erosion Behaviour of Turbine Rotor Blades Installed in the Krsko Nuclear Power Plant, *Wear*, 2003, **254**, p 735–741
16. T. Manisekaran, M. Kamaraj, S.M. Sharif, and S.V. Joshi, Slurry Erosion Studies on Surface Modified 13Cr-4Ni Steels: Effect of Angle of Impingement and Particle Size, *J. Mater. Eng. Perform.*, 2007, **16**(5), p 567–572
17. I·V. Rivero and C·O. Ruud, Residual Stresses and Patterns in 52100 Bearing Steel: Preliminary Analysis of Strain Hardening vs. Micro Structural Transformation by XRD Analysis, *J. Soc. Tribol. Lubr. Eng.*, 2002, **58**, p 30–40
18. J. Grum and R. Sturm, Deformation of Specimen During Laser Surface Remelting, *J. Mater. Eng. Perform.*, 2000, **9**(2), p 138–146